Solar Cells

How to cite:
International Edition: doi.org/10.1002/anie.202209580
German Edition: doi.org/10.1002/ange.202209580

Central Unit Fluorination of Non-Fullerene Acceptors Enables Highly Efficient Organic Solar Cells with Over 18 % Efficiency

Hongbin Chen[+], Huazhe Liang[+], Ziqi Guo, Yu Zhu, Zhe Zhang, Zhixiang Li, Xiangjian Cao, Haohui Wang, Wanying Feng, Yalu Zou, Lingxian Meng, Xiaoyun Xu, Bin Kan, Chenxi Li, Zhaoyang Yao, Xiangjian Wan, Zaifei Ma,* and Yongsheng Chen**

Abstract: Halogenation of terminal of acceptors has been shown to give dramatic improvements in power conversion efficiencies (PCEs) of organic solar cells (OSCs). Similar significant results could be expected from the halogenation of the central units of state-of-the-art Y-series acceptors. Herein, a pair of acceptors, termed CH6 and CH4, featuring a conjugation-extended phenazine central unit with and without fluorination, have been synthesized. The fluorinated CH6 has enhanced molecular interactions and crystallinity, superior fibrillar network morphology and improved charge generation and transport in blend films, thus affording a higher PCE of 18.33 % for CH6-based binary OSCs compared to 16.49 % for the non-fluorinated CH4. The new central site offers further opportunities for structural optimization of Y-series molecules to afford better-performed OSCs and reveals the effectiveness of fluorination on central units.

Introduction

Organic solar cells (OSCs) with successively increased power conversion efficiencies (PCEs) have been regarded as one of the most attractive technologies to generate renewable energies due to their intrinsic merits including low cost,[1] solution processing,[2] tunable transparency[3] and flexibility.[4] Recently, PCEs of over 18 % and 19 % for binary and ternary OSCs, respectively, have been afforded,[5] mainly resulting from extensive explorations of novel non-fullerene acceptors (NFAs) with acceptor-donor-acceptor (A-D-A) architectures.[6] Among them, OSCs based on the state-of-the-art Y-series NFAs could not only undergo a highly efficient charge generation with a very small driving force and greatly decreased energy loss (E_{loss}) even below 0.50 eV, but also have a suitable morphology in the blend films.[7] Although various chemical modifications have been performed on Y-series NFAs so far,[5a,8] morphology optimization via precise molecular structure designing to balance the trade-off between open circuit voltage (V_{OC}) and short circuit current density (J_{SC}),[9] at the same time, improve the fill factors (FFs) is still confronting great challenges.[5a,8d,10]

Halogenations have been extensively employed to modify light-harvesting molecules and thus given rise to significant performance improvement of OSCs.[11] The underlying reasons of introducing halogens to improve device performance could be taken into consideration from two aspects. Firstly, at single-molecular level, with the relatively high electronegativity but small steric hindrance, halogenation could (1) tune the energy levels and absorption of light-harvesting materials easily;[11a] (2) strengthen donor-acceptor (D-A) feature of molecules, thus contributing to an enlarged molar extinction coefficients and efficient intramolecular charge transfer (ICT).[6] On the other hand, at molecular packing level, halogenation could (1) strengthen intermolecular π–π stacking by increasing the planarity of molecules or/and enhancing intermolecular non-covalent bond interactions;[8d,12] (2) regulate molecular packing modes and crystallization, thus controlling/optimizing molecular aggregation behaviors.[8d,11a] All the above factors could combine together to render a better film morphology generally, being in favor of efficient exciton dissociations, enhanced charge transfer/transport, suppressed recombination and thus improved photovoltaic performances of OSCs.

As regard to NFAs like ITIC[13] or F analogs,[14] the main intermolecular packing mode is "end unit to end unit",[7a] which can be observed from their corresponding single crystals. Therefore, it is understandable that halogenation engineering is mostly performed on end units to enable more suitable film morphologies, improved photodynamic processes and enlarged PCEs of OSCs. However, in sharp

[*] H. Chen,[+] H. Liang,[+] Z. Guo, Y. Zhu, Z. Zhang, Z. Li, X. Cao, H. Wang, W. Feng, Y. Zou, L. Meng, B. Kan, C. Li, Z. Yao, X. Wan, Y. Chen
State Key Laboratory and Institute of Elemento-Organic Chemistry, The Centre of Nanoscale Science and Technology and Key Laboratory of Functional Polymer Materials, Renewable Energy Conversion and Storage Center (RECAST), College of Chemistry, Nankai University
Tianjin 300071 (China)
E-mail: zyao@nankai.edu.cn
yschen99@nankai.edu.cn
X. Xu, Z. Ma
State Key Laboratory for Modification of Chemical Fibers and Polymer Materials, Center for Advanced Low-dimension Materials, College of Materials Science and Engineering, Donghua University
Shanghai 201620 (China)
E-mail: mazaifei@dhu.edu.cn
[+] These authors contributed equally to this work.

contrast to the major packing mode of "end unit to end unit" in ITIC or F analogs, it is worth noting that central units (for example, benzothiadiazole in Y6)[15] have also been involved in molecular packings significantly and led to an effective 3D intermolecular packing network for state-of-the-art Y-series NFAs.[5a,7a,8c,9b] This unique 3D intermolecular packing network could not only boost efficient charge separation/transport, but also suppress charge recombination.[11b,16] That is why the champion PCE of over 19 % has be achieved with a much smaller E_{loss}, which in turn highlights the dominant role of central unit in such highly efficient OSC's molecular packing.[5a,7a] In light of the great success achieved by halogenations on end units, further improvement of OSCs could also be expected, if performing suitable halogenation on the central units of the already highly performed Y-series NFAs could be achieved. Nevertheless, it is really interesting to note that the halogenations of Y-series NFAs has been still focused on end units[7b,11a] or side chains[17] extensively. This largely unexplored halogenations on central units might partially be caused by the absence of reactive sites on benzothiadiazole central unit in current Y6 analogs, but more importantly, the huge challenges of constructing other new central heterocyclic units.

Bearing these thoughts in mind, we believe that it is quite meaningful to construct some other new central heterocyclic units with halogenations on them and further reveal their largely unexplored but crucial role in tuning molecular packing, optimizing film morphology to improve the overall performance of OSCs. Therefore, two NFAs (CH4 and CH6) with A-D-A feature have been constructed with the same backbones, both featured with π extension in the central unit constructed by phenazine conversion from benzothiadiazole with respect to Y6,[7b] where CH6 has the fluorination on the newly constructed central unit, compared with CH4 without the fluorination (Figure 1a). The newly emerging phenazine central units in CH4 and CH6 are constructed conveniently through an efficient in situ phenazine conversion from benzothiadiazole, thus affording a universal method to further construct some other exotic central heterocyclic units.[7a] With respect to that of CH4, CH6 with extra fluorinations on central unit demonstrates down-shifted energy levels, stronger molecular π–π interaction, increased crystallinity and thus superior fibrillar network morphology. As a result, benefiting from the enhanced charge generation/transport and lower energy disorder, a much higher PCE of 18.33 % with a V_{OC} of 0.875 V, J_{SC} of 26.62 mA cm^{-2} and an excellent fill factor (FF) of 78.4 % can be achieved for CH6-based binary OSCs, compared to that of a PCE of 16.49 %, a V_{OC} of 0.888 V, a J_{SC} of 26.11 mA cm^{-2} and a relatively low FF of 71.1 % for CH4-based binary OSCs. Moreover, an excellent PCE of 16.52 % with a V_{OC} of 0.873 V, J_{SC} of 25.43 mA cm^{-2} and FF of 74.4 % can be also achieved by CH6-based OSCs with 1 cm^2 active area, qualifying as one of the best 1 cm^2 OSCs thus far.[8a,18] Our work has afforded a method to construct novel central units with more chemical active sites and reveals the crucial role of central unit fluorination in boosting PCEs of OSCs, especially for the state-of-the-art Y-series NFAs.

Results and Discussion

The extra fluorinations on central unit should have an effect on the frontier molecular orbitals of NFAs, thus density functional theory (DFT) calculation was firstly resorted to unveil the variation of energy levels, orbital distributions, etc. As shown in Figure 1b, after fluorination on central unit of phenazine, an obvious dipole moment of 2.38 Debye can be afforded for the central unit comparing to that of 0 Debye without fluorination, which is due to the huge electronegativity of fluorine atoms. Meanwhile, due to the large electronegativity of fluorine atoms, an increased electrostatic surface potential of 2,3-difluorophenazine and the both down-shifted highest occupied molecular orbitals (HOMOs) and lowest unoccupied molecular orbitals (LUMOs) energy levels for CH6 can been observed, comparing to that of CH4.[19] As a result, the HOMO and LUMO energy levels of CH6 downshift by 70 and 50 meV, respectively, with respect to that of CH4 (Figure S1). Note that the relatively larger change of HOMO is caused by the fluorination on central unit, while relatively smaller impact was observed on the LUMOs. This is also consistent with the clear A-D-A feature of CH4 and CH6, which can be indicated by the characteristic peak-valley-peak plots for their frontier orbital charge density differences (ΔQ) on molecular backbone in the longest direction (Figure 1c and Figure S2).[6] As it has been proposed before, such an A-D-A feature of NFAs could endow NFAs with enhanced molecular packing, better exciton separation and charge transport, smaller energy losses, and thus greatly improved performance for OSCs compared with other types of molecules.[6]

The synthetic routes to CH4 and CH6 were displayed in Figure 1d and Scheme S1. The detailed procedures and characterizations were described in Supporting Information. Taking the donor construction of CH4 as an example (Figure 1d), the challenging but indispensable conversion of phenazine from benzothiadiazole was generally achieved by an in situ method through two unstable intermediates **1a** and **1b**,[7a] which provides a novel route to further construct some other exotic central heterocyclic units. In details, a feasible reductive reaction was conducted firstly to generate intermediate **1a**, which could undergo a subsequent oxidation reaction to yield intermediate **1b** due to the highly electron-rich feature of **1a**. At last, a condensation between **1b** and commercially available benzene-1,2-diamine could afford the donor of CH4 with an excellent overall yield of 81 %.

In order to evaluate the experimental energy levels of CH4 and CH6, the cyclic voltammetry (CV) has been conducted (Figure S3 and S4). As shown in Figure 1e, both HOMO and LUMO energy levels of CH6 downshift due to the large electronegativity of fluorine atoms, being −5.68 and −3.85 eV respectively, comparing to that of −5.64 and −3.83 eV for CH4. Note that the relative alignment of frontier molecular orbital energy levels obtained from CVs are consistent well with that predicted by DFT calculations (Figure S1). The maximum absorption peaks of CH6 in dilute chloroform solution and neat film locate at 742 and

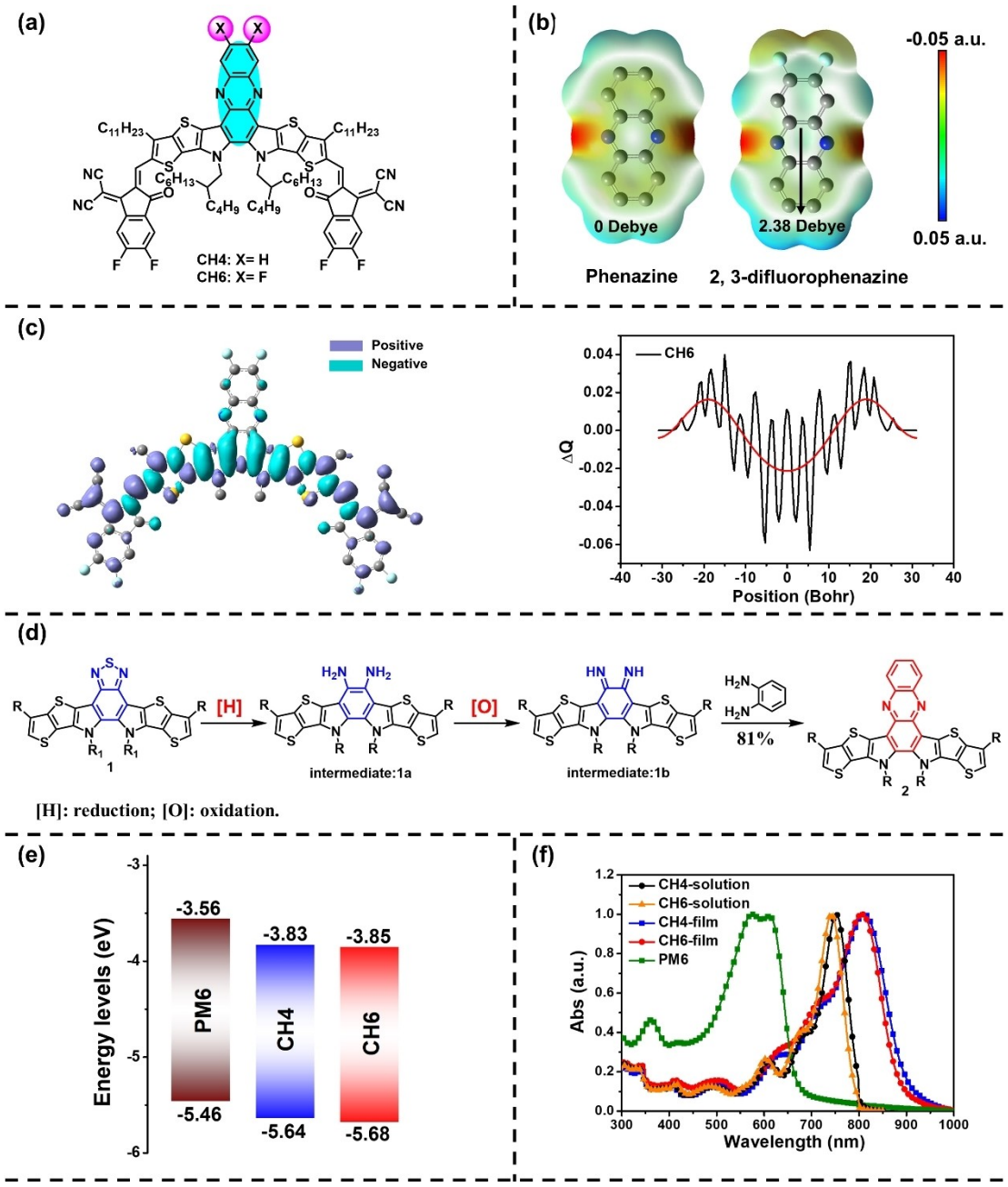

Figure 1. a) Molecular structures of CH4 and CH6. b) electrostatic surface potential (ESP) maps of central units for CH4 and CH6. c) Theoretical density distribution ΔQ ($\Delta Q = \Psi^2_{LUMO} - \Psi^2_{HOMO}$) along the longest axis (backbone) of CH6. d) Synthesized route to the key central unit of CH4. e) Energy level diagram of PM6, CH4 and CH6 derived from CVs. f) Normalized absorption spectra.

806 nm, respectively, blue-shifting by 10 and 5 nm with respect to that of 752 nm in solution and 811 nm in solid film for CH4 (Figure 1f). This should be attributed to the electron-withdrawing fluorine atoms on central unit of CH6, which downshifts the HOMO energy level significantly and gives rise to a larger energy band gap of 1.83 eV than that of 1.81 eV for CH4 derived from CVs. More interestingly, an obviously larger redshift ($\Delta\lambda$) of 64 nm has been observed when varying from solution to film for CH6 with respect to that of 59 nm for CH4, indicating the stronger intermolecular π–π stacking caused by fluorination on central unit.[20] In addition, the relatively sharp absorption edge for CH6 in low energy region can be indicated by the enlarged slope (−0.014 for CH6 and −0.012 for CH4), suggesting a lower energy disorder in blend films which will be further discussed below.[21] Moreover, both CH4 and CH6 exhibit an excellent thermal stability with a decomposition temperature over 330 °C, measured by the thermal gravimetric analysis (TGA) (Figure S5). The corresponding detailed physicochemical data was summarized in Table S1.

To further evaluate the influence of fluorination on central unit on device performance, OSCs with a conven-

tional architecture of ITO Glass/PEDOT:PSS/BHJ layer/PNDIT-F3N/Ag have been fabricated. Among them, polymeric donor PM6[22] (Figure S6) with matched energy levels and complementary absorption (Figure 1e and 1f) was selected to blend with CH4 and CH6. A champion PCE of 18.33 % was afforded by CH6 based OSCs along with a V_{OC} of 0.875 V, J_{SC} of 26.62 mA cm^{-2} and FF of 78.4 % (Figure 2a and Table 1), much better than that of 16.49 % for its CH4 counterpart which has a slightly larger V_{OC} of 0.888 V but inferior J_{SC} of 26.11 mA cm^{-2} and FF of 71.1 %. Figure 2b displays the PCE distribution histogram of 15 independently measured OSCs (detailed device parameters in Table S2 and S3), exhibiting the evidently higher average PCEs for CH6 based OSCs. Note that the approximate 20 % improvement in PCE has been achieved by CH6 based OSCs compared with that of CH4, which should mainly be contributed to its significantly improved J_{SC} and FF. Although the blue-shifted absorption of CH6 renders a slight narrower range of external quantum efficiencies (EQEs) spectra (Figure 2c), the overall higher EQE values, especially in low energy region, still render a larger integrated current density of 25.87 mA cm^{-2} for CH6 based OSCs compared to that of 25.45 mA cm^{-2} for CH4 based one. The $\approx$0.5 mA cm^{-2} enlarged integrated J_{SC} for CH6 based OSCs comparing to that of CH4 is in good agreement with the J_{SC} derived from J–V curves in Figure 2a. The enlarged EQE values of CH6

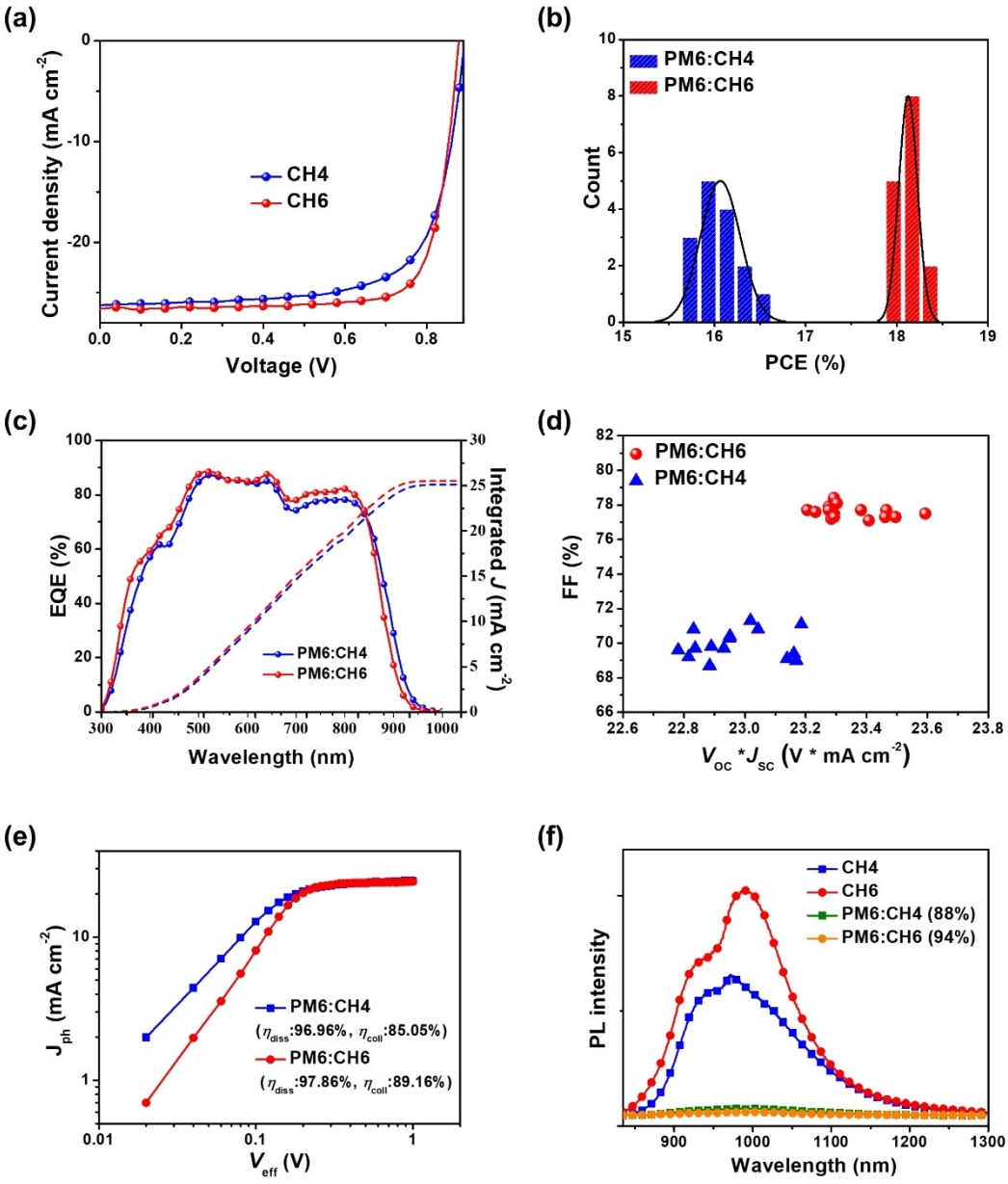

Figure 2. a) J–V curves of the devices based on PM6:CH4 and PM6:CH6. b) Histogram of the PCEs of OSCs, fitted with Gaussian distributions (solid lines). c) EQE curves of the devices based on PM6:CH4 and PM6:CH6. d) V_{OC}×J_{SC} vs FF of CH6 based and CH4 based 15 independently measured OSCs. e) J_{ph} versus V_{eff} curves. f) Photoluminescence spectra of neat and blend films.

Table 1: Summary of device parameters for optimized OSCs.[a]

Active layer	V_{OC} [V]	J_{SC} [mA cm^{-2}]	Calc. J_{SC}[b] [mA cm^{-2}]	FF [%]	PCE [%]
PM6:CH4	0.888 (0.888 ± 0.003)	26.11 (25.87 ± 0.16)	25.45	71.1 (69.9 ± 0.7)	16.49 (16.06 ± 0.17)
PM6:CH6	0.875 (0.878 ± 0.001)	26.62 (26.56 ± 0.09)	25.87	78.4 (77.6 ± 0.3)	18.33 (18.12 ± 0.08)

[a] Statistical and optimal results are listed in parentheses and outside of parentheses, respectively. The average parameters were calculated from 15 independent devices. [b] Current densities calculated from EQE curves.

should be ascribed to the more efficient charge generation/collection discussed below. As will be also discussed below in details, the simple fluorination on central unit of CH6 has caused more ordered molecular packing, leading to lower energy disorder and an increased charge mobility, all of which should account for the greatly improved FF for CH6 based OSCs. In addition, the slightly inferior V_{OC} of CH6 based OSCs is consisted with its downshifted LUMO energy level comparing to that of CH4 (Figure 1e). As presented intuitively in Figure 2d, a remarkable improvement of $V_{OC} \times J_{SC}$ for CH6 based OSCs indicates that a more balanced trade-off between V_{OC} and J_{SC} has been achieved.

Given the great importance of large-area processing in industrial applications, OSCs with 1 cm^2 active area were also fabricated based on CH6. By using the same fabricating condition with small devices, an excellent PCE of 16.52 % with a V_{OC} of 0.873 V, J_{SC} of 25.43 mA cm^{-2} and FF of 74.4 % can be achieved, qualifying as one of the best 1 cm^2 OSCs thus far.[8a,18] The corresponding *J–V* and EQE curves were presented in Figure S7.

As we have discussed above, fluorinations on central unit could result in a much better device performance, which should be determined by the related superior light dynamic processes in OSCs. Therefore, the charge generation, transport and recombination behaviors in both CH4 and CH6 based devices were also characterized. As displayed in Figure 2e, CH6 based OSC could afford an excellent exciton dissociation efficiency (P_{diss}) of 97.86 % and charge collection efficiency (P_{coll}) of 89.16 %, both of which are better than that of 96.96 % for P_{diss} and 85.05 % for P_{coll} in the CH4 control devices.[23] This partially accounts for the enlarged EQE values for CH6 based OSCs mentioned above. The improved P_{diss} in CH6 based OSCs may be determined by the downshifted HOMO energy level of CH6, which gives rise to a larger driving force in theory for exciton dissociation.[24] This is also consistent with the higher photoluminescence quenching yield (η_{PLQ}) of 94 % for PM6:CH6 blends compared with that of 88 % for PM6:CH4 (Figure 2f). Whereas the greatly enlarged P_{coll} should be attributed to the higher and more balanced μ_e/μ_h ratio for PM6:CH6 blends (Figure S8 and Table S4).[25] Based on the space-charge limited current (SCLC) model, CH6 based device shows both higher hole/electron mobilities of $2.58 \times 10^{-4}/4.19 \times 10^{-4}$ cm^2 V^{-1} s^{-1} than those of $1.50 \times 10^{-4}/3.05 \times 10^{-4}$ cm^2 V^{-1} s^{-1} for CH4, further affording a more balanced μ_e/μ_h ratio of 1.62 for PM6:CH6 blend with respect to that of 2.03 for PM6:CH4 blend (Figure S8 and Table S4). In addition, from the dependence of J_{SC} and V_{OC} on light intensity in Figure S9, the $S/(kT/q)$ (1.14 for CH4 and 1.13 for CH6) and α (0.982 for CH4 and 0.987 for CH6) are quite similar and near to unit, indicating the charge recombination in blend films was suppressed significantly.[23,26] The detailed photodynamic parameters were summarized in Table S4.

In light of the dominant role of film morphologies in achieving favorable photodynamic in OSCs, Grazing incident wide-angle X-ray scattering (GIWAXS) measurements were performed to unveil the molecular packing behaviors and orientations (Figure 3a and b).[27] Given that central units in Y-series NFAs have been verified to participate in molecular packing extensively,[7a,15a] thereby it can be expected that fluorinations on central unit of CH6 could also make a difference in molecular packings. As illustrated in Table S5, both CH4 and CH6 neat and blend films displayed a strong (010) diffraction peak in out-of-plane (OOP) direction and a (100) diffraction peak in in-plane (IP) direction, suggesting both the preferable face-on molecular stacking orientation. Note that the (010) diffraction peak in OOP direction for PM6:CH6 blend locates at 1.73 Å^{-1} with a smaller π–π packing distance of 3.63 Å than that of 3.76 Å (corresponding to a diffraction peak of 1.67 Å^{-1}) for PM6:CH4 blend, suggesting fluorinations on central units could enhance molecular π–π stacking and further facilitate intermolecular charge transfers. The enlarged crystal coherence length (CCL) of 24.5 Å for (010) diffraction peak in OOP direction and 78.5 Å for (100) diffraction peak in IP direction can be achieved by PM6:CH6 blend, with respect to that of 19.1 and 60.8 Å for PM6:CH4 blend, respectively. The more ordered molecular packing or better crystallinity for CH6 should be caused by fluorinations on central unit and also in good accordance with the larger slope afforded by the UV/Vis spectrum (Figure 1f) and increased root-mean square (RMS) roughness of 0.93 nm (0.81 nm for CH4 blends) observed from atomic force microscopy (AFM) images in Figure 3c.[28] In addition, a clear fibrillar network morphology of PM6:CH6 blend can be observed, which may contribute to the more efficient charge generation/transport and thus improved J_{SC} and FF for CH6 based OSCs as we have discussed above,[29] demonstrating the vital role of fluorinations on central unit in morphology optimization. Furthermore, the slightly reduced miscibility between CH6 and PM6 donor than that of CH4 evaluated by their Flory-Huggins interaction parameter χ (0.27 and 0.22 for CH6 and CH4 based systems, respectively, see Figure S10 and Table S6 for the details)

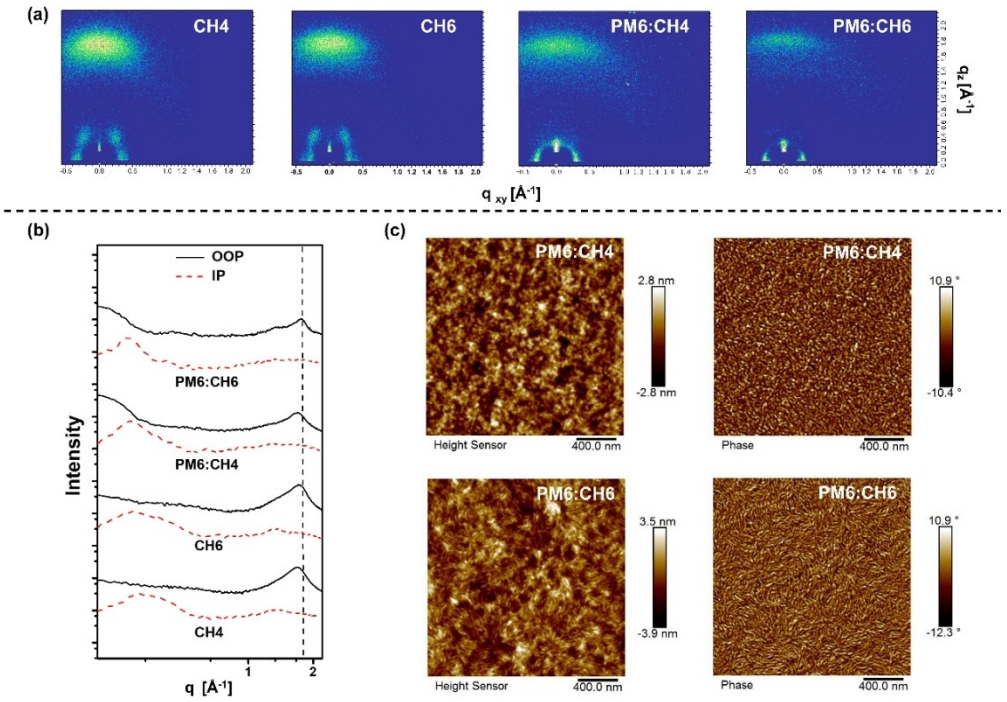

Figure 3. a) 2D GIWAXS patterns and b) corresponding 1D line-cuts of optimized CH4 and CH6 based neat and blend films. c) AFM height and phase images CH4 and CH6 based blend films.

also indicates the improved crystallinity for CH6 caused by fluorinations on central units.[30]

In order to investigate the influence of central unit fluorination on E_{loss} of OSCs, the detailed energy loss analysis of CH4 and CH6 based OSCs were carried out. As presented in Figure 4a, the total E_{loss} can be determined by the following equation: $E_{loss}=E_g-qV_{OC}$ (E_g represents the optical band gap and q is the elementary charge) and divided into three parts: ΔE_{CT}, $q\Delta V_r$ and $q\Delta V_{nr}$.[31] Among them, ΔE_{CT} is the energetic difference between the singlet excited and charge-transfer (CT) states, which is essential for the efficient exciton separation. $q\Delta V_r$ and $q\Delta V_{nr}$ represented the inevitable radiative and non-radiative recombination energy losses, respectively. The detailed data of ΔE_{CT}, $q\Delta V_r$ and $q\Delta V_{nr}$ were measured and summarized in Table S7 and the details of measured method were described in Supporting Information.

By analyzing the cross-point of normalized PL and UV/Vis spectra of neat films,[32] E_g can be estimated as 1.40 and 1.41 eV for CH4 and CH6, respectively (Figure S11). In combination with V_{OC}s of OSCs, the corresponding total E_{loss}es can be determined to be 0.51 eV for PM6:CH4 based OSCs and 0.53 eV for PM6:CH6 based one (Figure 4b). The similar E_{loss}es of CH4 and CH6 based OSCs make them ranking among the smallest E_{loss} systems,[5,7,8a] especially in high-efficiency PCE systems,[5a,7a] indicating great potentials for further structural or device optimization to improve the PCEs of resulting OSCs.

As it is well known, EQE spectra in low energy region are determined by the absorption of CT states, thus the E_{CT}s of CH4 and CH6 based OSCs can be estimated to be 1.36 and 1.35 eV, respectively, by fitting the corresponding highly sensitive EQEs (sEQE) and electroluminescence (EL) spectra (Figure 4c and d).[31] The corresponding ΔE_{CT} can be afforded through the equation: $\Delta E_{CT}=E_g-E_{CT}$, being 0.04 and 0.06 eV for CH4 and CH6, respectively. Note that the larger ΔE_{CT} of CH6 based OSC could usually afford a larger driving force for exciton separation in theory,[31a] which is consisting with its higher charge generation efficiency analyzed above. Nevertheless, based on the recently developed three-state model,[33] a smaller ΔE_{CT} may contribute to a potential hybridization between local exciton (LE) and CT states and thus resulting in a relatively lower non-radiative recombination rate for CT state through a possible mechanism of intensity borrowing or the energy transfer from CT to LE states.[34] As a result, $q\Delta V_{nr}$ for CH4 based OSCs is slightly lower than that of CH6 based one (0.21 vs 0.23 eV for CH4 and CH6, respectively), as indicated by the lower EQE_{EL} values of 0.87×10^{-4} for CH6 with respect to that of 2.33×10^{-4} for CH4 based devices (Figure S12). Furthermore, the slightly suppressed $q\Delta V_r$ (0.25 eV) for CH6 comparing to CH4 (0.26 eV) based devices should be ascribed to the lower energetic disorder for PM6:CH6 blend,[21,35] which can be indicated by the decreased Urbach energy (E_U) values of 21.2 meV for PM6:CH6, comparing to that of 22.3 meV for PM6:CH4 (Figure S13). Note that the lower E_U for PM6:CH6 blend than that of PM6:CH4 is also in accordance with its sharper absorption edge (Figure 1f), enlarged CCL and enhanced crystallization. Generally, although the total E_{loss} of OSCs based on CH6 with central unit fluorinations enlarged slightly with respect to that of OSCs based on CH4, a better trade-off between tangle J_{SC} and V_{OC} can be

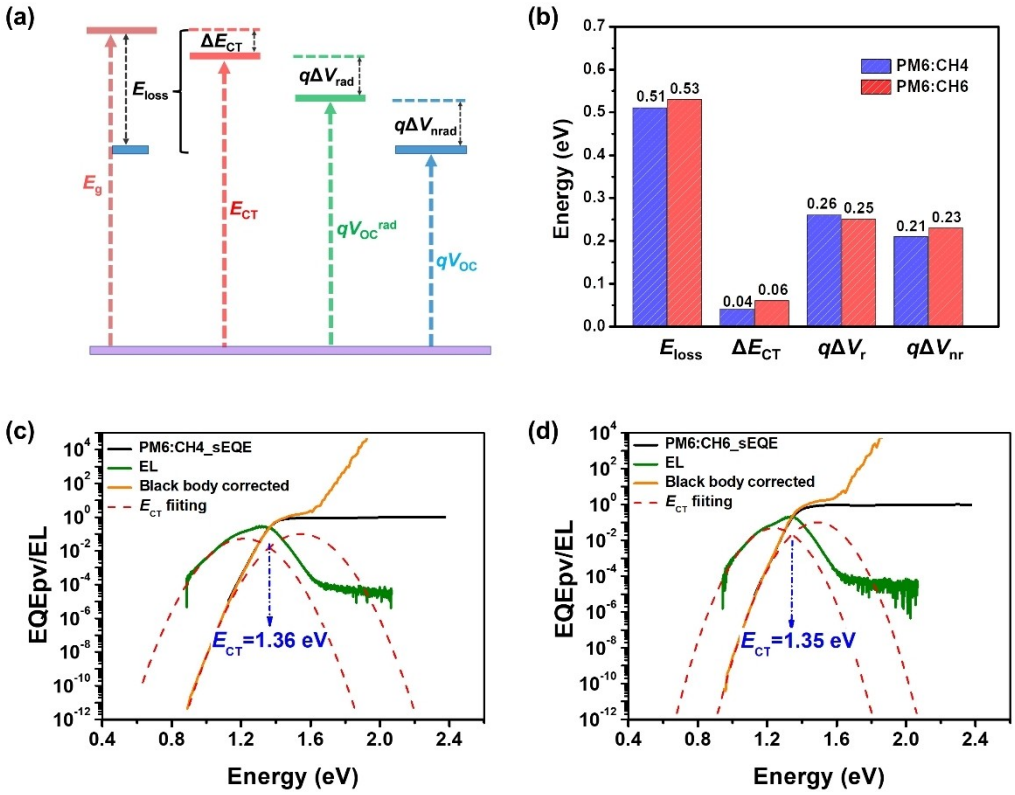

Figure 4. a) A schematic diagram of E_{loss} related parameters. b) Detailed E_{loss} of CH4 and CH6 based devices. c) and d) Sensitive external quantum efficiency (sEQE) spectra and the fitting results for the relevant devices.

still achieved due to the superior film morphology for CH6. As a result, a much higher PCE for CH6 based OSCs was afforded along with a greatly improved FF, highlighting the great potential of central unit halogenations to further boost device performances.

Furthermore, considering possible fitting error of CT state in high-efficiency NFA-based OPV system without obvious CT-state features, we also categorized E_{loss} into three contributions ($E_{loss}=\Delta E_1+\Delta E_2+\Delta E_3$) based on the SQ limit theory which does not directly depend on CT-state energy.[32,36] Among them, ΔE_1 and ΔE_2 are the radiative recombination energy losses above and below the band gap of the active layer,[32] respectively. ΔE_3 represents the non-radiative recombination energy losses, which is relevant to $q\Delta V_{nr}$ mentioned above.[31b] The detailed data of ΔE_1, ΔE_2 and ΔE_3 were measured and summarized in Table 2 and the details of measured method were described in Supporting Information. Based on Table 2, we can find that ΔE_1 (0.26 eV) and ΔE_2 (0.04 eV) are the same for both the CH4 and CH6 based solar cells. As a result, the slightly lower E_{loss} for OSC based on PM6:CH4 than that of PM6:CH6 based one should be mainly due to the reduced non-radiative recombination energy losses (ΔE_3). which is consistent with the discussed results concluded by fitting CT state above.

Conclusion

Two A-D-A type NFAs termed CH4 and CH6 have been constructed with the same backbones, but fluorination only

Table 2: Total energy loss values and different contributions in solar cells based on the SQ limit theory.

Active layer	V_{oc} [V]	E_g[a] [eV]	V_{OC}^{SQ}[b] [V]	V_{OC}^{rad}[b] [V]	ΔE_1[c] [eV]	ΔE_2[d] [eV]	ΔE_3[e] [eV]	E_{loss}[f] [eV]
PM6:CH4	0.89	1.40	1.14	1.10	0.26	0.04	0.21	0.51
PM6:CH6	0.88	1.41	1.15	1.11	0.26	0.04	0.23	0.53

[a] E_g is estimated by the cross-point of normalized absorption and emission spectra of neat film. [b] V_{OC}^{SQ} is the upper limit for the V_{oc} of the solar cell derived in the Shockley–Queissier theory. V_{OC}^{rad} is the radiative recombination limit for the V_{oc} of the solar cell, which can be determined by the equation:[32] $V_{OC}^{SQ}=\frac{kT}{q}\ln\left(\frac{J_{SC}^{SQ}}{J_0^{SQ}}+1\right)\cong\frac{kT}{q}\ln\left(\frac{q\bullet\int_{E_g}^{+\infty}\phi_{AM1.5G}(E)dE}{q\bullet\int_{E_g}^{+\infty}\phi_{BB}(E)dE}\right)$ and $V_{OC}^{rad}=\Delta E_3/q+V_{oc}$; [c] $\Delta E_1=E_g-qV_{OC}^{SQ}$; [d] $\Delta E_2=qV_{OC}^{SQ}-qV_{OC}^{rad}$; [e] $\Delta E_3=kTln\left(\frac{1}{EQE_{EL}}\right)$;[31b] EQE_{EL} values for CH6 and CH4 based devices is 0.87×10^{-4} and 2.33×10^{-4}, respectively. [f] $E_{loss}=\Delta E_1+\Delta E_2+\Delta E_3$.[32]

of the central unit of CH6, affords a platform with multiple chemical modification sites for further structural optimization on the state-of-the-art Y-series NFAs to construct better-performed OSCs. A systematic investigation revealed the dominant role of fluorination of the central units (not only of end groups) in I) tuning molecular energy levels effectively; II) forming superior fibrillar network film morphologies through enhancing intermolecular π–π interaction, increasing molecular packing order and crystallinity; III) facilitating efficient charge generation/transport in blend films with a lower energy disorder; and IV) addressing the trade-off among tangle J_{SC} and V_{OC}, and also improving FF to achieve high-performance OSCs. As a result, a PCE of 18.33 % was achieved by CH6 based binary OSCs compared to that of 16.49 % for CH4 without central-unit fluorination. Moreover, a high PCE of 16.52 % can be further afforded by CH6 based OSCs with 1 cm^2 active area, demonstrating the great prospects in large-area devices for industrial application. Our work highlights the effectiveness of halogenation of central units, especially for the state-of-the-art Y-series NFAs, to boost PCEs of OSCs and will stimulate the further explorations for novel heterocyclic central units with halogen substitution.

Acknowledgements

The authors gratefully acknowledge the financial support from NSFC (21935007, 52025033, 51873089, 52073056) and MoST (2019YFA0705900) of China, Tianjin city (20JCZDJC00740), 111 Project (B12015), the 100 Young Academic Leaders Program of Nankai University (020-ZB22000110 and 020-92220002) and Haihe Laboratory of Sustainable Chemical Transformations.

Conflict of Interest

The authors declare no conflict of interest.

Data Availability Statement

The data that support the findings of this study are available in the Supporting Information of this article.

Keywords: Central Unit · Fluorination · Non-Fullerene Acceptor · Solar Cells · Y-series

[1] C. Yang, S. Zhang, J. Ren, M. Gao, P. Bi, L. Ye, J. Hou, *Energy Environ. Sci.* **2020**, *13*, 2864–2869.
[2] S. Dong, T. Jia, K. Zhang, J. Jing, F. Huang, *Joule* **2020**, *4*, 2004–2016.
[3] W. Liu, S. Sun, L. Zhou, Y. Cui, W. Zhang, J. Hou, F. Liu, S. Xu, X. Zhu, *Angew. Chem. Int. Ed.* **2022**, *61*, e202116111; *Angew. Chem.* **2022**, *134*, e202116111.
[4] G. Zeng, W. Chen, X. Chen, Y. Hu, Y. Chen, B. Zhang, H. Chen, W. Sun, Y. Shen, Y. Li, F. Yan, Y. Li, *J. Am. Chem. Soc.* **2022**, *144*, 8658–8668.
[5] a) C. Li, J. Zhou, J. Song, J. Xu, H. Zhang, X. Zhang, J. Guo, L. Zhu, D. Wei, G. Han, J. Min, Y. Zhang, Z. Xie, Y. Yi, H. Yan, F. Gao, F. Liu, Y. Sun, *Nat. Energy* **2021**, *6*, 605–613; b) L. Zhu, M. Zhang, J. Xu, C. Li, J. Yan, G. Zhou, W. Zhong, T. Hao, J. Song, X. Xue, Z. Zhou, R. Zeng, H. Zhu, C.-C. Chen, R. C. I. MacKenzie, Y. Zou, J. Nelson, Y. Zhang, Y. Sun, F. Liu, *Nat. Mater.* **2022**, *21*, 656–663.
[6] X. Wan, C. Li, M. Zhang, Y. Chen, *Chem. Soc. Rev.* **2020**, *49*, 2828–2842.
[7] a) H. Chen, Y. Zou, H. Liang, T. He, X. Xu, Y. Zhang, Z. Ma, J. Wang, M. Zhang, Q. Li, C. Li, G. Long, X. Wan, Z. Yao, Y. Chen, *Sci. China Chem.* **2022**, *65*, 1362–1373; b) J. Yuan, Y. Zhang, L. Zhou, G. Zhang, H.-L. Yip, T.-K. Lau, X. Lu, C. Zhu, H. Peng, P. A. Johnson, M. Leclerc, Y. Cao, J. Ulanski, Y. Li, Y. Zou, *Joule* **2019**, *3*, 1140–1151.
[8] a) Y. Cui, H. Yao, J. Zhang, K. Xian, T. Zhang, L. Hong, Y. Wang, Y. Xu, K. Ma, C. An, C. He, Z. Wei, F. Gao, J. Hou, *Adv. Mater.* **2020**, *32*, 1908205; b) K. Jiang, Q. Wei, J. Y. L. Lai, Z. Peng, H. K. Kim, J. Yuan, L. Ye, H. Ade, Y. Zou, H. Yan, *Joule* **2019**, *3*, 3020–3033; c) F. Lin, K. Jiang, W. Kaminsky, Z. Zhu, A. K. Y. Jen, *J. Am. Chem. Soc.* **2020**, *142*, 15246–15251; d) X. Zhang, G. Li, S. Mukherjee, W. Huang, D. Zheng, L.-W. Feng, Y. Chen, J. Wu, V. K. Sangwan, M. C. Hersam, D. M. DeLongchamp, J. Yu, A. Facchetti, T. J. Marks, *Adv. Energy Mater.* **2022**, *12*, 2102172.
[9] a) Y. Su, L. Zhang, Z. Ding, Y. Zhang, Y. Wu, Y. Duan, Q. Zhang, J. Zhang, Y. Han, Z. Xu, R. Zhang, K. Zhao, S. Liu, *Adv. Energy Mater.* **2022**, *12*, 2103940; b) C. Yang, Q. An, H.-R. Bai, H.-F. Zhi, H. S. Ryu, A. Mahmood, X. Zhao, S. Zhang, H. Y. Woo, J.-L. Wang, *Angew. Chem. Int. Ed.* **2021**, *60*, 19241–19252; *Angew. Chem.* **2021**, *133*, 19390–19401; c) T. Liu, R. Ma, Z. Luo, Y. Guo, G. Zhang, Y. Xiao, T. Yang, Y. Chen, G. Li, Y. Yi, X. Lu, H. Yan, B. Tang, *Energy Environ. Sci.* **2020**, *13*, 2115–2123.
[10] a) Y. Yan, Y. Zhang, Y. Liu, Y. Shi, D. Qiu, D. Deng, J. Zhang, B. Wang, M. A. Adil, K. Amin, W. A. Memon, M. Wang, H. Zhou, X. Zhang, Z. Wei, *Adv. Energy Mater.* **2022**, *12*, 2200129; b) H. Meng, C. Liao, M. Deng, X. Xu, L. Yu, Q. Peng, *Angew. Chem. Int. Ed.* **2021**, *60*, 22554–22561; *Angew. Chem.* **2021**, *133*, 22728–22735.
[11] a) L. Wang, Q. An, L. Yan, H.-R. Bai, M. Jiang, A. Mahmood, C. Yang, H. Zhi, J.-L. Wang, *Energy Environ. Sci.* **2022**, *15*, 320–333; b) S. Li, L. Zhan, N. Yao, X. Xia, Z. Chen, W. Yang, C. He, L. Zuo, M. Shi, H. Zhu, X. Lu, F. Zhang, H. Chen, *Nat. Commun.* **2021**, *12*, 4627; c) L. Zhan, S. Li, Y. Li, R. Sun, J. Min, Z. Bi, W. Ma, Z. Chen, G. Zhou, H. Zhu, M. Shi, L. Zuo, H. Chen, *Joule* **2022**, *6*, 662–675.
[12] a) H. Chen, H. Lai, Z. Chen, Y. Zhu, H. Wang, L. Han, Y. Zhang, F. He, *Angew. Chem. Int. Ed.* **2021**, *60*, 3238–3246; *Angew. Chem.* **2021**, *133*, 3275–3283; b) C. Li, X. Zhang, N. Yu, X. Gu, L. Qin, Y. Wei, X. Liu, J. Zhang, Z. Wei, Z. Tang, Q. Shi, H. Huang, *Adv. Funct. Mater.* **2022**, *32*, 2108861; c) X. Zhou, S. Pang, B. Wu, J. Zhou, H. Tang, K. Lin, Z. Xie, C. Duan, F. Huang, Y. Cao, *ACS Appl. Energy Mater.* **2022**, *5*, 7710–7718; d) T.-J. Wen, J. Xiang, N. Jain, Z.-X. Liu, Z. Chen, X. Xia, X. Lu, H. Zhu, F. Gao, C.-Z. Li, *J. Energy Chem.* **2022**, *70*, 576–582.
[13] a) T. J. Aldrich, M. Matta, W. Zhu, S. M. Swick, C. L. Stern, G. C. Schatz, A. Facchetti, F. S. Melkonyan, T. J. Marks, *J. Am. Chem. Soc.* **2019**, *141*, 3274–3287; b) Y. Lin, J. Wang, Z.-G. Zhang, H. Bai, Y. Li, D. Zhu, X. Zhan, *Adv. Mater.* **2015**, *27*, 1170–1174.
[14] a) X. Ke, L. Meng, X. Wan, M. Li, Y. Sun, Z. Guo, S. Wu, H. Zhang, C. Li, Y. Chen, *J. Mater. Chem. A* **2020**, *8*, 9726–9732; b) N. Qiu, H. Zhang, X. Wan, C. Li, X. Ke, H. Feng, B. Kan, H. Zhang, Q. Zhang, Y. Lu, Y. Chen, *Adv. Mater.* **2017**, *29*, 1604964.

[15] a) G. Zhang, X.-K. Chen, J. Xiao, P. C. Y. Chow, M. Ren, G. Kupgan, X. Jiao, C. C. S. Chan, X. Du, R. Xia, Z. Chen, J. Yuan, Y. Zhang, S. Zhang, Y. Liu, Y. Zou, H. Yan, K. S. Wong, V. Coropceanu, N. Li, C. J. Brabec, J.-L. Bredas, H.-L. Yip, Y. Cao, *Nat. Commun.* **2020**, *11*, 3943; b) L. Zhu, M. Zhang, G. Zhou, T. Hao, J. Xu, J. Wang, C. Qiu, N. Prine, J. Ali, W. Feng, X. Gu, Z. Ma, Z. Tang, H. Zhu, L. Ying, Y. Zhang, F. Liu, *Adv. Energy Mater.* **2020**, *10*, 1904234.
[16] Z. Zhou, W. Liu, G. Zhou, M. Zhang, D. Qian, J. Zhang, S. Chen, S. Xu, C. Yang, F. Gao, H. Zhu, F. Liu, X. Zhu, *Adv. Mater.* **2020**, *32*, 1906324.
[17] K. Chong, X. Xu, H. Meng, J. Xue, L. Yu, W. Ma, Q. Peng, *Adv. Mater.* **2022**, *34*, 2109516.
[18] Y. Han, Z. Hu, W. Zha, X. Chen, L. Yin, J. Guo, Z. Li, Q. Luo, W. Su, C.-Q. Ma, *Adv. Mater.* **2022**, *34*, 2110276.
[19] Y. Cui, P. Zhu, X. Liao, Y. Chen, *J. Mater. Chem. C* **2020**, *8*, 15920–15939.
[20] T.-J. Wen, Z.-X. Liu, Z. Chen, J. Zhou, Z. Shen, Y. Xiao, X. Lu, Z. Xie, H. Zhu, C.-Z. Li, H. Chen, *Angew. Chem. Int. Ed.* **2021**, *60*, 12964–12970; *Angew. Chem.* **2021**, *133*, 13074–13080.
[21] J. Yuan, C. Zhang, B. Qiu, W. Liu, S. K. So, M. Mainville, M. Leclerc, S. Shoaee, D. Neher, Y. Zou, *Energy Environ. Sci.* **2022**, *15*, 2806–2818.
[22] M. Zhang, X. Guo, W. Ma, H. Ade, J. Hou, *Adv. Mater.* **2015**, *27*, 4655–4660.
[23] A. K. K. Kyaw, D. H. Wang, V. Gupta, W. L. Leong, L. Ke, G. C. Bazan, A. J. Heeger, *ACS Nano* **2013**, *7*, 4569–4577.
[24] B. Kan, J. Zhang, F. Liu, X. Wan, C. Li, X. Ke, Y. Wang, H. Feng, Y. Zhang, G. Long, R. H. Friend, A. A. Bakulin, Y. Chen, *Adv. Mater.* **2018**, *30*, 1704904.
[25] X. Zhang, C. Li, J. Xu, R. Wang, J. Song, H. Zhang, Y. Li, Y.-N. Jing, S. Li, G. Wu, J. Zhou, X. Li, Y. Zhang, X. Li, J. Zhang, C. Zhang, H. Zhou, Y. Sun, Y. Zhang, *Joule* **2022**, *6*, 444–457.
[26] L. J. A. Koster, V. D. Mihailetchi, R. Ramaker, P. W. M. Blom, *Appl. Phys. Lett.* **2005**, *86*, 123509.
[27] P. Müller-Buschbaum, *Adv. Mater.* **2014**, *26*, 7692–7709.
[28] Y. Huang, E. J. Kramer, A. J. Heeger, G. C. Bazan, *Chem. Rev.* **2014**, *114*, 7006–7043.
[29] Q. Liu, Y. Jiang, K. Jin, J. Qin, J. Xu, W. Li, J. Xiong, J. Liu, Z. Xiao, K. Sun, S. Yang, X. Zhang, L. Ding, *Sci. Bull.* **2020**, *65*, 272–275.
[30] S. Nilsson, A. Bernasik, A. Budkowski, E. Moons, *Macromolecules* **2007**, *40*, 8291–8301.
[31] a) H. Liu, M. Li, H. Wu, J. Wang, Z. Ma, Z. Tang, *J. Mater. Chem. A* **2021**, *9*, 19770–19777; b) K. Vandewal, K. Tvingstedt, A. Gadisa, O. Inganäs, J. V. Manca, *Phys. Rev. B* **2010**, *81*, 125204.
[32] Y. Wang, D. Qian, Y. Cui, H. Zhang, J. Hou, K. Vandewal, T. Kirchartz, F. Gao, *Adv. Energy Mater.* **2018**, *8*, 1801352.
[33] X.-K. Chen, D. Qian, Y. Wang, T. Kirchartz, W. Tress, H. Yao, J. Yuan, M. Hülsbeck, M. Zhang, Y. Zou, Y. Sun, Y. Li, J. Hou, O. Inganäs, V. Coropceanu, J.-L. Bredas, F. Gao, *Nat. Energy* **2021**, *6*, 799–806.
[34] F. D. Eisner, M. Azzouzi, Z. Fei, X. Hou, T. D. Anthopoulos, T. J. S. Dennis, M. Heeney, J. Nelson, *J. Am. Chem. Soc.* **2019**, *141*, 6362–6374.
[35] a) Z. Zhang, Y. Li, G. Cai, Y. Zhang, X. Lu, Y. Lin, *J. Am. Chem. Soc.* **2020**, *142*, 18741–18745; b) S. Liu, J. Yuan, W. Deng, M. Luo, Y. Xie, Q. Liang, Y. Zou, Z. He, H. Wu, Y. Cao, *Nat. Photonics* **2020**, *14*, 300–305.
[36] J. Liu, S. Chen, D. Qian, B. Gautam, G. Yang, J. Zhao, J. Bergqvist, F. Zhang, W. Ma, H. Ade, O. Inganäs, K. Gundogdu, F. Gao, H. Yan, *Nat. Energy* **2016**, *1*, 16089.

Manuscript received: June 30, 2022
Accepted manuscript online: July 27, 2022
Version of record online: ■■, ■■

Research Articles

Solar Cells

H. Chen, H. Liang, Z. Guo, Y. Zhu, Z. Zhang, Z. Li, X. Cao, H. Wang, W. Feng, Y. Zou, L. Meng, X. Xu, B. Kan, C. Li, Z. Yao,* X. Wan, Z. Ma,* Y. Chen* _____ e202209580

Central Unit Fluorination of Non-Fullerene Acceptors Enables Highly Efficient Organic Solar Cells with Over 18% Efficiency

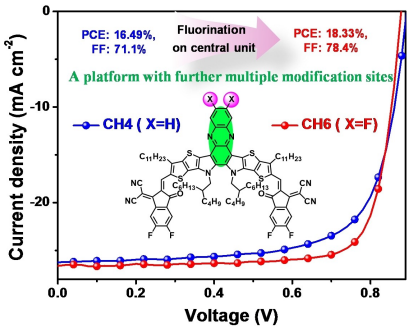

A series of CH molecules with newly modification site on central unit of Y-series electron acceptors has been designed and synthesized to afford better-performed organic solar cells (OSCs). Further fluorination on the largely unexplored central unit enabled significantly improved photovoltaic performance with over 18% efficiency for CH6-based binary OSCs..